Possible Atmosphere and Ionospheric Anomalies of the 2019 Pakistan Earthquake Using Statistical and Machine Learning Procedures on MODIS LST, GPS TEC, and GIM TEC

Amna Hafeez, Munawar Shah ⓘ, Muhsan Ehsan, Punyawi Jamjareegulgarn ⓘ, Junaid Ahmed, M. Arslan Tariq, Shahid Iqbal, and Najam Abbas Naqvi

Abstract—Identifying atmospheric and ionospheric anomalies based on remote sensing satellites has contributed highly to develop the hypothesis of lithosphere-atmosphere-ionosphere coupling over the earthquake (EQ) epicenter during the seismic preparation period. This article has investigated the variations of potential EQ precursor in daytime and nighttime land surface temperature (LST) before and after the 2019 Pakistan EQ from Moderate Resolution Imaging Spectroradiometer (MODIS) satellite. The nighttime LST values of MODIS exhibit temporal anomalies during nighttime period within a time window of five days before and after the main shock day. Furthermore, the LST values predicted by artificial neural network (ANN) validate the significant enhancement in nighttime time series of MODIS. The nighttime LST anomalies obtained from the observation and ANN prediction are more than 20% and 7% of normal distribution beyond the confidence bounds, respectively, within five days after the main shock. Likewise, the ionospheric anomaly from daily total electron content (TEC) values at Sukkur Global Positioning System (GPS) station confirms the EQ associated ionospheric perturbations on the day after the main shock. The Global Ionospheric Maps (GIMs) also show the TEC anomalies during 1000–1400 LT on September 25, 2019.

Index Terms—Earthquake, global ionospheric map (GIM) total electron content (TEC), Global Positioning System (GPS) TEC, lithosphere-atmosphere-ionosphere coupling, moderate resolution imaging spectroradiometer (MODIS) land surface temperature (LST).

Amna Hafeez, Munawar Shah, and Najam Abbas Naqvi are with the Department of Space Science Space Education, GNSS Lab National Center of GIS and Space Application, Institute of Space Technology, Islamabad 44000, Pakistan (e-mail: amnahafeez016@gmail.com; shahmunawar1@gmail.com; najam.naqvi@ist.edu.pk).

Muhsan Ehsan is with the Department of Earth and Environmental Sciences, Bahria University, Islamabad 44000, Pakistan (e-mail: muhsanehsan98@hotmail.com).

Punyawi Jamjareegulgarn is with the King Mongkut's Institute of Technology Ladkrabang, Prince of Chumphon Campus, Chumphon 86160, Thailand (e-mail: kjpunyaw@gmail.com).

Junaid Ahmed and M. Arslan Tariq are with the Centre for Earthquake Studies, National Centre for Physics, Islamabad 44000, Pakistan (e-mail: junaid.ahmed@ncp.edu.pk; arslan@ncp.edu.pk).

Shahid Iqbal is with the Department of Earth Sciences, Quaid e Azam University, Islamabad 15320, Pakistan (e-mail: shahid_lefty@hotmail.com).

Digital Object Identifier 10.1109/JSTARS.2021.3119382

I. INTRODUCTION

THE space-based earthquake (EQ) precursors have emerged as a significant field to search the possible anomalies of the seismic event over the epicenter during the preparation period [1], [2]. Moreover, the remote sensing satellites have been employed in several applications for the observation of different events such as EQ, planetary surfaces, and atmosphere phenomena, etc. [3], and they have also provided more benefits over the conventional methods to monitor proper estimation of the EQ precursors. Hence, they can provide adequate measurement to detect seismic hazards forecasting. In contrast, the ground-based seismic stations for EQ monitoring are fairly rare as compared to different remote sensing satellites for the monitoring of seismic events. For instance, the usage of thermal remote sensing has carried out the novel trends in EQ research with high resolution long-and short-term datasets [4]. More analyses for possible EQ precursor can also be done using the ionospheric data from Detection of Electro-Magnetic Emissions Transmitted from Earthquake Regions, Swarm satellites, and Global Positioning System (GPS). Potential EQ precursors include cloud formation, weather patterns change, air temperature, abnormal land surface temperature (LST), and ionosphere variations [5].

The EQ is a kind of mechanical process, which occurs due to sudden energy burst in the earth's lithosphere at the seismogenic zone and activates seismic energy to outer atmosphere. Consequently, it could result in various thermal and ionospheric anomalies. Stressed buildings before an EQ event in tectonically active regions enhance the ground temperature near the lithosphere-atmosphere interface, then follow by energy emanation to atmosphere and lower ionosphere as a result of complex ions and molecules reactions. The satellite-based thermal anomalies offer significant evidences about EQ precursors [4], [5]. Freund *et al.* [5] discovered that the positive holes [p-holes] were generated from stressed rocks inside the hypocentral region as a result of tectonic forces. Due to the upward migration of p-holes over the epicenter, the complex reactions and the air ionization transfer lithospheric energy to atmosphere that disturb the upper atmosphere and ionosphere. Furthermore, the p-holes trigger variations on lithosphere LST and also alter the normal travel path of radio signal in the upper atmosphere and

ionosphere. Moreover, Pulinets and Ouzounov [6] reported that radon emanation from the seismogenic zone transports seismic energy to litosphere-atmosphere interface during EQ preparation period in lithosphere-atmosphere-ionosphere coupling (LAIC) coupling model. Subsequently, this radon rises upward to different altitude in atmosphere and causes upward drift of abnormal atomspheric heating to ionosphere.

Among different EQ precursors, the satellite-based pre/co/postseismic thermal anomalies and ionosphere perturbations associated with main shocks have been studied in different reports [7], [8], [26]. They observed the EQs of different magnitudes all over the world and confirmed the EQ associated total electron content (TEC) variations using GNSS observations. In general, the thermal anomalies are considered to be one of the EQ precursors, which is an unexpected increase in LST during the seismic preparation period, and they are analyzed in spatial LST images of on-board satellites to monitor the EQ energy emanation. A change in epicentral thermal temperature can be sensed by different on-board satellites such as Moderate Resolution Imaging Spectroradiometer (MODIS) and AVHRR [1]. The spatial and temporal variations of thermal anomalies associated with EQ are correlated in different ways with impending main shocks under the LAIC mechanism. The thermal anomalous association with several major EQs have been reported in different case studies [1], [9]. Moreover, LST data retrieved from different satellites and other atmospheric and ionospheric products are the most useful datasets for demonstrating the EQ precursors [1].

In this article, we have investigated seismic-induced thermal and ionospheric anomalies before and after the Pakistan EQ that hits the Mirpur region in Azad Kashmir on September 24, 2019. The LST data extracted from MODIS are used to investigate the Pakistan EQ during daytime and nighttime periods for two months before and two months after the EQ. Moreover, both the TEC values from GPS (hereafter, GPS TEC) of Sukkur station and the TEC values obtained from Global Ionosphere Map (hereafter, GIM TEC) are studied for the same EQ to delineate the LAIC hypothesis. The main goals of this article are as follows: 1) to point out a window for EQ precursors in MODIS LST, GPS TEC and GIM TEC, and 2) to enlighten the performance of different methods on LST time series to verify the EQ induced thermal anomalies such as statistical calculation and ANN model. More analyses are conducted in this article in order to validate and confirm the seismic induced ionospheric thermal anomalies of the 2019 Pakistan EQ. The rest of this article is organized as follows. Section II describes the study area and Section III is dedicated to the used data and methods. The results and discussions are addressed in Section IV. Finally, Section V concludes this article.

II. STUDY AREA

The Kashmir EQ with a shallow hypocentral depth 10 km struck the Pakistani region on September 24, 2019 at 16:02 local time (11:02 UTC). Its epicenter was located at 7 km SSE of Mirpur, Pakistan (33.1°N, 73.7°E). The maximum felt intensity of VII (very strong) on the Modified Mercalli scale was announced by the United State Geological Survey (USGS).

There were severe damages to lives and infrastructure in Mirpur District, for instance, culminating in the deaths of 40 people and more than 850 people were injured. Moreover, several bridges and roads were completely demolished, particularly within 14 km of the main seismogenic region. The epicenter of the EQ was 3 km south of new Mirpur city and 20 km north of the Jhelum city. The EQ is caused by the movement of the reverse Jari Kass fault in the Mirpur region where it has many active fault splays. A shallow blind fault line is outlined, fetching both the Jari Kass fault line and the Samwal fault on the surface exposition of this blind fault line. Moreover, the low magnitude EQs as aftershock series have continued in the Mirpur region after restoring of the Mangla repository. Along these fault lines, there is a likelihood that the uprising may have enhanced the hydrostatic pressure that have been activating increment in the strain build up [10].

Another possible cause of this EQ is the result of a shallow reverse faulting close to the Indian and Eurasian plates. Focal mechanism provisions are not all around compelled yet showing regularly the invert slip on a shallow or steeply plunging fault (e.g., USGS). Shallow east–west striking converse faulting is steady with the tectonics of the area [11]. The EQs and the active faults in northern Pakistan and the adjacent parts of India and Afghanistan are the immediate outcomes of this impact. In addition, the boundary delivers the most elevated mountain tops in the world including the Karakoram, Himalayan, the Pamir, and the Hindu Kush ranges. As the Indian plate moves toward the north, it is being subducted or pushed underneath the Eurasian plate. It is recognized that the Indian plate converges with the Eurasian plate at a pace of 39 mm/year at the site of this event. More information about this EQ is available on the USGS web site.[1]

III. USED DATA AND METHODS

The MODIS LST images used in this article are retrieved from the earth observing system flagship satellite "Terra" that was launched by the National Aeronautics and Space Administration (NASA) on December 18, 1999. MODIS LST product from Terra has been provided to scientific community since February, 2000. Note that Terra has a sun-synchronous, nearly polar, and circular orbit, which passes from north to south above the earth [12]. It passes the earth's equator at 10:30 local time in the morning and the revisit period is 1-2 days around the earth. Terra has five important sensors that observe the ocean, atmosphere, land, and ice for many scientific purposes (for example, MO-PITT, CERES, ASTER, MISR, and MODIS). MODIS captures 36 discrete spectral bands with bandwidth of 0.415–14.235 μm in the electromagnetic spectrum. MODIS observations provide surface emissivity and LSTs in 7 thermal infrared bands in the form of pairs (nighttime and daytime) of maps. The MODIS products include LSTs, view angles, observation time, quality assessment, and emissivity [12].

In addition, the daily day and nighttime LST images assembled as MOD11A1 (V6) [27] are downloaded from USGS

---

[1][Online]. Available: https://earthquake.usgs.gov/earthquakes/eventpage/us60005mqp/executive

earth explorer for the time interval of 2 months before and 2 months after the 2019 Pakistan EQ. These images provide daily emissivity and LST. The LST product files consist of the global attributes (metadata) as well as the scientific datasets (arrays) with local attributes, as shown in the web page.[2] The missing values of LST under cloud cover over the epicenter are retrieved via Random Forest technique, as shown in Zhao et al. [24]. More details about reconstruction of LST under cloud cover are in Zhao and Duan [25]. Then, the LST is validated by GPS TEC anomalies from Sukkur station inside the Dobrovolsky *et al.* [13] region. Moreover, the LST values are obtained from MODIS over the epicentral Latitude and Longitude.

In this article, the daily GPS TEC values at Sukkur station are also used to study the ionospheric variations over the epicenter of the 2019 Pakistan EQ. Here, the GPS TEC values before and after the main shock are analyzed in the form of vertical TEC (VTEC) along the line of sight from satellite to receiver station. The VTEC values are shown in TEC unit (1 TECU = 10^{16} el/m^2). Here, the STECs (slant TECs) are used to derive the VTEC values as given, respectively, in

$$\text{STEC}_a^h = \frac{-(f_1^2 f_2^2)}{40.3(f_1^2 - f_2^2)}(P_{(4,a)}^h - c.\text{DCB}_a - c.\text{DCB}^h) \tag{1}$$

$$\text{VTEC} = \text{STEC} \times \cos\left(\arcsin\left(\frac{\text{Rsinz}}{\text{R} + \text{H}}\right)\right) \tag{2}$$

where (f_1, f_2) are dual frequencies of GPS system, c is the speed of light, $P_{(4,a)}^h$ is the differences between smoothed coded measurements, DCB_a and DCB^h are differential code biases for satellite and GPS receiver, respectively, H is the ionospheric height which of 350 km, R is the earth's radius, and z is the zenith angle of the satellite. The GPS TEC and MODIS LST data are calculated in the critical zone of the seismogenic region. It is very important to conduct the precursory studies within an effective zone around the EQ epicenter, where epicenter as a focal point. The radius of the seismogenic zone (unit: km) is determined from Dobrovolsky *et al.* [13]

$$\rho = 10^{0.43 \times M} \tag{3}$$

where M is the EQ magnitude. Equation (3) shows that the EQs with high magnitude have a large critical zone and vice versa.

Furthermore, the EQ induced variations over the epicenter on are also investigated using the abnormal VTEC from bihourly GIM TEC maps. Note that the spatial resolution of the GIM TEC map is 2.5° along latitude and 5° in longitude direction and its temporal resolution is bihourly. The spatial mean LST values are computed for 2 months before and 2 months after the main shock day during daytime and nighttime periods. The spatial images during September 21–28, 2019 are also analyzed to confirm the EQ-induced variations over the epicenter in the lower atmosphere to validate the variations of temporal analysis. Subsequently, the spatial LST maps are prepared with a view angle-dependent algorithm applied to direct observations during daytime and nighttime periods [14].

TABLE I
OBSERVED ATMOSPHERIC-IONOSPHERIC ANOMAILIES

Data	Anomalous Day			Anomalous Night		
	Pre-EQ	Post-EQ	Deviation	Pre-EQ	Post-EQ	Deviation
MODIS LST	Nil	Nil	Nil	Nil	+1	17.68°C
GPS TEC	Nil	+1	> 8TECU	Nil	Nil	Nil
GIM TEC	Nil	+1	> 8TECU	Nil	Nil	Nil

To find abnormal variations in both LST and GPS TEC values, a statistical analysis on the basis of mean and standard deviation is also applied on the available data before and after the main shock. The confidence bounds for an observed LST and GPS TEC values are determined from the mean and standard deviation (σ) of ten days before and after the event of observed day. The values above or below the confidence bounds are considered as anomalies. Here, the upper (UB) and lower (LB) bounds are indicated by the following equations [1]:

$$\text{UB} = \bar{\text{X}} + 2\sigma \tag{4}$$

$$\text{LB} = \bar{\text{X}} - 2\sigma. \tag{5}$$

In order to confirm the EQ precursors, ANN predicted LST anomalies are also calculated to connect the LAIC phenomena over the epicenter. ANN is used to show a complex connection between input and output parameters for discovering the anomalous pattern in the data. Theoretically, a simplified structure of ANN consists of three types of layers (i.e., input, hidden, and output layers), where each layer has several neurons depending upon the specified application. One layer is connected to next layer by direct links and weights representing specific outgoing signal strengths. The ANN inputs in the proposed method consist of the average LST values, LST pixel values, latitude, longitude, time in days, and deviations. Whereas, the output is days of the year including EQ occurrence day. Then, abnormality of LST was observed on the basis of comparison between ANN predicted LST and measured MODIS LST. Both the LST values and the spatially average LST values are retrieved over the epicenter of the 2019 Pakistan EQ. The ANN can be used to detect the abnormal LST values of MODIS associated with the main shock of impending EQ [1], [15]. The procedure encompasses the training phase (training a network) with a bulk of sample of representative data, after which one exposes the network to data for the validation or prediction phase to predict the new outcomes.

IV. RESULTS AND DISCUSSION

A. Results

The 2019 Pakistan EQ (M_w 5.6) hits the different parts of Pakistan and neighboring countries including India and Afghanistan with a shallow hypocentral depth of 10 km. For possible EQ precursors, the data of MODIS LST, GPS TEC, and GIM TEC are analyzed to monitor the atmospheric and ionospheric anomalies within the critical zone of this main shock (see Table I). We find that the ionospheric anomalies can be seen clearly in the data
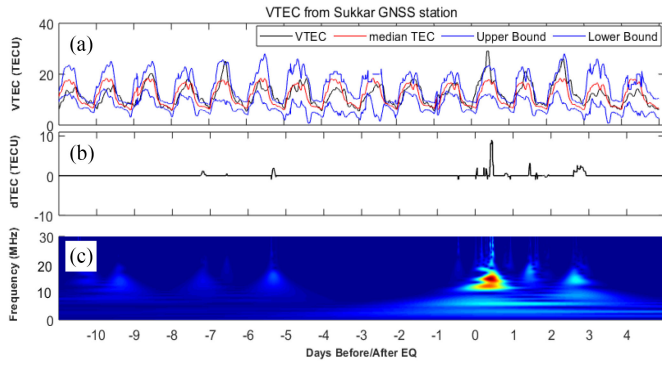
Fig. 1. (a) VTEC, and (b) dTEC values obtained from GNSS receiver at Sukkar station during 10 days before and 5 days after the main shock day (September 24, 2019) of the Mw 5.6 Pakistan EQ. (c) Clear EQ-induced thermal anomaly is shown in the frequency spectrum.

of Sukkur GPS station after one day of the main shock during the daytime period. Consequently, the anomalous variations in VTEC can be found obviously, as shown in Fig. 1(a), in which it corresponds to the post-seismic energy emanation into ionosphere. Fig. 1(b) and (c) shows the variation in differential TEC (dTEC), which is larger than 8 TECU after the main shock and the abnormal TEC has a frequency spectrum of 20 MHz for this EQ-induced anomaly.

Fig. 2 depicts the spatial TEC maps obtained from GIMs to verify the abnormal TEC cloud on September 25, 2019 (a day after the main shock) over the epicenter. The red filled star in Fig. 2 represents the epicenter region and LT stands for local time, which is bihourly for every GIM map. The abnormal TEC clouds over epicenter during daytime 0800-1200 LT confirm the coupling of lithosphere and atmosphere to travel up to ionosphere. More analysis of GIM TEC shows that EQ-induced electron density initiates at 0800 LT and lingers the epicenter till 1200 LT, as shown in Figs. 2(d)–(f). Subsequently, the maximum electron density clouds start to move away from the epicenter from 1400 LT onwards, as illustrated in Fig. 2(g)–(l). All these anomalies in GPS TEC and GIM TEC prompt the discussion that seismic activity exports energy to the atmosphere and ionosphere in the form of p-holes [16] and other gases (like radon, etc.) [6]. However, both the hypotheses (p-holes and radon emanation) need further investigations with more equipped satellite instruments. In addition, the abnormal gases cause air ionization at the earth-atmosphere interface and p-holes rise up to high altitudes in the ionosphere to form seismo-induced ionospheric anomalies. The ionospheric anomalies probably rise up over the epicenter region via atmospheric medium during the EQ preparation period. For this purpose, thermal anomalies from MODIS LST are studied to reveal the LAIC mechanism.

More evidences are investigated in the statistical analysis and ANN based LST enhancement and depletion within the EQ preparation zones to locate the LAIC mechanism. Fig. 3 shows the daytime LST values (unit: °C) between July 20, 2019 and November 20, 2019 in the form of average daytime LST values, an upper bound, and lower bound are represented by blue, green, and orange lines, respectively. Fig. 3(b) and (c) shows the corresponding deviations and percentage deviations (unit: %) with

respect to the confidence bounds, respectively. The red dash line represents the main shock day on September 24, 2021, and the confidence bounds are the upper and the lower bounds computed by (4) and (5), respectively. As shown in Fig. 3, the daytime LST values from MODIS shows no significant enhancement or depletion within the period of two months before and after the main shock. A low depletion far beyond the main shock after more than one month (LST < 1 °C) can be observed, but it has no relation with the EQ as found in Fig. 3(b) and (c). Due to low intensity and distant occurrence from the EQ day, the daytime LST anomaly is omitted. However, we emphasized in this article that LAIC coupling can be possible within 5–10 days before the EQ or 5–10 days after the main shock. Particularly, the low intense anomalies in space measurements are false indicators in different datasets.

In addition, it can be seen clearly that both no spatial enhancement in daytime LST maps and the variations of less than 5 °C occur over epicentral lineament regions, as illustrated in Fig. 4. The daytime spatial LST maps show quiet LST in daily MODIS images before and after the main shock day (September 24, 2019), which correlate completely with the temporal analysis in Fig. 3. The average temperature rises up between 1 °C and 3 °C in spatial LST maps, however, no noticeable change occurs in temporal analysis to identify the abnormal seismic event during daytime period. This could be due to the fact that the intense radiative heat around the epicenter settles no significant LST variation during daytime period. The daytime LST is more tightly coupled with the radiative and thermodynamic characteristics of the earth's surface than the standard air temperature measurements [17]. On the other hand, the analysis of daytime MODIS LST reported by Sekertekin *et al.* [1] showed LST increment significantly with respect to the EQ epicenter.

Fig. 5 illustrates the comparison of daytime LST values (unit: °C) during 2 months before and 2 months after the main shock day of the studied Pakistan EQ as well as the deviations (unit: %) between the observed and ANN predicted LST values. It can be seen that during daytime period, both the observed and ANN predicted LST values have no significant LST enhancement (no

EQ anomaly) around the main shock day of the M$_w$ 5.6 Pakistan EQ, which endorses the absence of enhancement in spatial LST maps and temporal LST values during daytime period. On the other hand, nighttime LST variation after the main shock day (probable postseismic thermal responses) is clearly visible beyond the upper bound, as shown in Fig. 6. The nighttime anomalous value is 6 times more than the normal distribution after the main shock day, as found in Fig. 6(b).

Previously, there are numerous physical explanations for postseismic thermal anomaly during nighttime period, and postseismic thermal responses are also found in this article. For instance, during nighttime period, the thermal anomaly looks like typical thermal anomaly, which is caused by the vertical distribution of air temperature. Moreover, due to topography and cloud shadow regions, the nighttime spatial imagery tends to avoid differential solar heating. The nighttime data also calms the chances of partial sun illumination, thus pointing the spatial thermal anomaly response [18]. Afterwards, Ouzounov
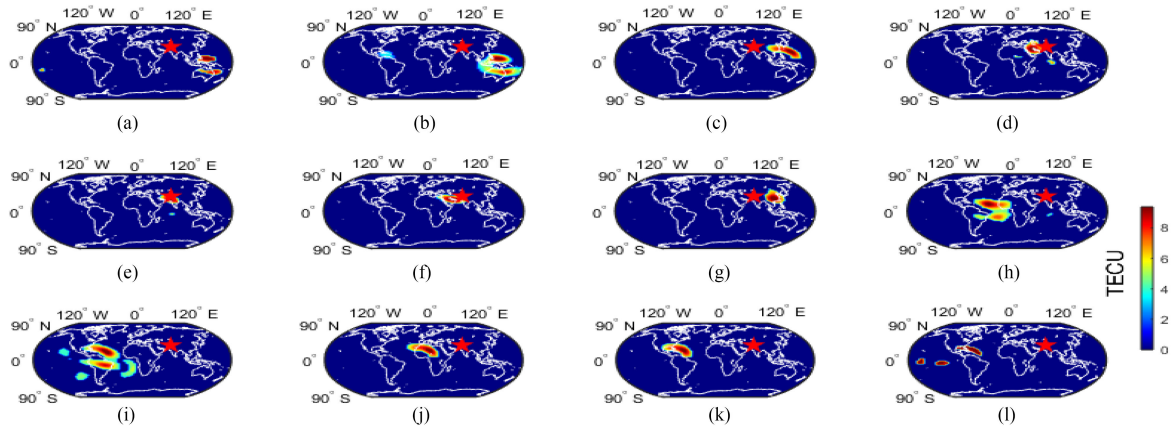
Fig. 2. Spatial TEC maps obtained from GIMs for an anomalous day of September 25, 2019 over the epicenter of the main shock. The red filled star represents the epicenter region and LT stands for local time, which is bihourly for every GIM map.
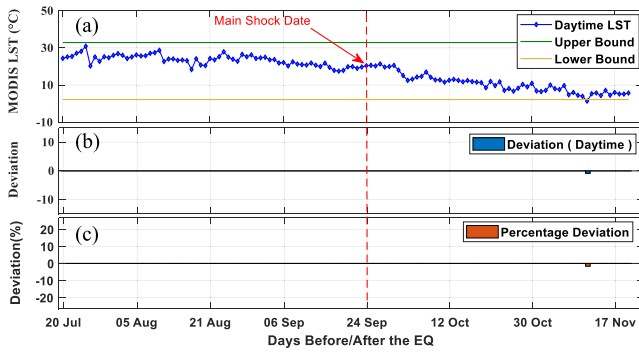

Fig. 3. Daytime LST values. Average daytime LST, an upper bound, and lower bound are represented by blue, green, and orange lines, respectively. (b) Deviations with respect to the confidence bounds. (c) Percentage deviations with respect to the confidence bounds.

Fig. 5. (a) Comparison of daytime LST (°C) during 2 months before and 2 months after the main shock date of the M_w 5.6 Pakistan EQ. (b) Deviations (%) between the statistically computed and ANN predicted LSTs.
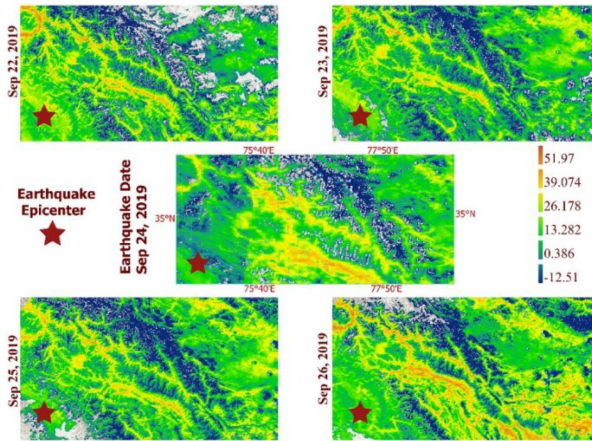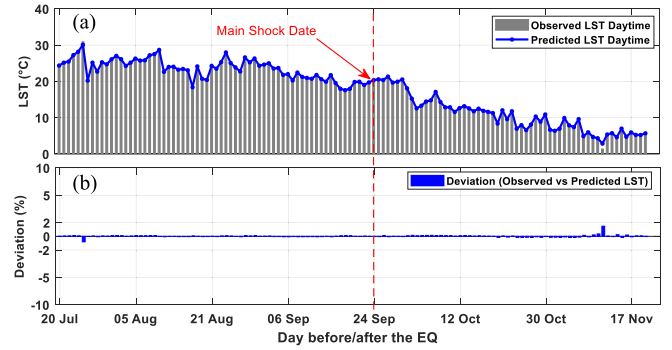

Fig. 4. Daytime spatial LST maps over the epicenter before and after the main shock date (September 24, 2019). Here, the red filled stars show the epicenter region.
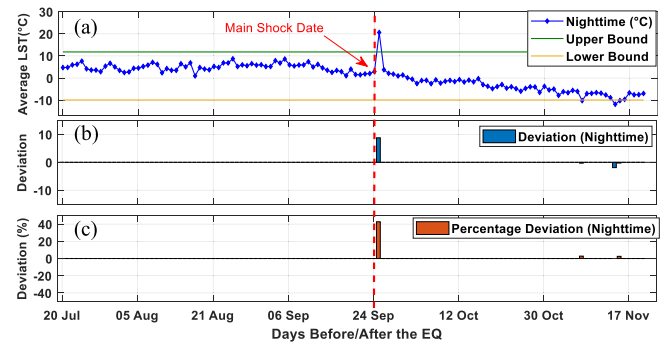

Fig. 6. (a) Average nighttime LST estimation, upper bound, and lower bound are represented by blue, green, and orange lines, respectively. (b) and (c) Their deviations and the percentage deviations, respectively.

et al. [19] reported that around neighboring areas of the EQ epicenter, the high tectonic stresses release greenhouse gases and radon that escape to the lower atmosphere, and infrared emission from the rock surface also augment the LST anomaly. Similarly, Dunajecka and Pulinets [20] discovered that radon

originating from crust of the earth causes air ionization and leads to a chain of physiochemical process that changes air molecule composition along with air temperature and humidity in LAIC hypothesis. Also, Pulinets et al. [21] verified the anomalies of air temperature and humidity related with the epicenter of EQ based on thorough multiparameter examination around the time of Colima EQ. For further investigation of the possibilities of LST increment, Ma et al. [22] assessed and suggested that the differences in temperature are associated with strain changes
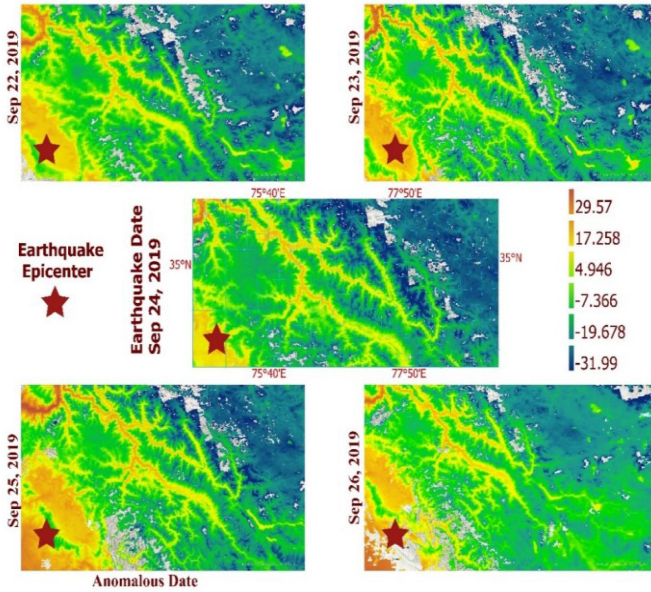
Fig. 7. Nighttime spatial LST maps over the epicenter before and after the main shock date (September 24, 2019) with highest anomaly on September 25, 2019. Here, the red filled stars show the epicenter.
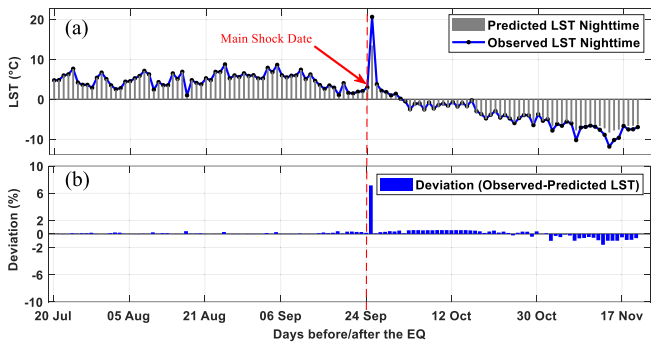

Fig. 8. (a) ANN predicted and observed nighttime LST values during 2 months before and 2 months after the Mw 5.6 Pakistan EQ. (b) Deviations between the statistically observed and ANN predicted LST values.

in the elastic deformation state, which exhibits temperature increment.

Fig. 7 depicts the spatial nighttime LST maps over the epicenter region (red filled stars) before and after the main shock day (September 24, 2019). We find that the highest anomalous variation of >10.71 °C can be seen immediately after the EQ during on September 25, 2019. Particularly, the significant rise in temperature as a result of abnormal emanation of energy reaches up to 20.60 °C. The nighttime LST anomaly of 8.796 °C with respect to the confidence bounds is more than 20% of the normal LST distribution in the deviation analysis. It is noteworthy that both spatial and temporal LST anomalies are discovered clearly, which validates more gas exhalation to confirm the LAIC phenomena and assists in the development of ionospheric anomalies at lower and upper edges of the ionosphere.

Similarly, the nighttime LST values are trained and predicted by ANN approach. Fig. 8(a) and (b) shows the nighttime LST values, which are obtained from the statistical observation and

ANN-based prediction during 2 months before and 2 months after the M$_w$ 5.6 Pakistan EQ, and their corresponding deviations. The nighttime deviations between the observed LST values and ANN predicted LST values are also computed to differentiate the thermal responses triggered by the EQ. During ANN analysis of nighttime data, we attained average temperature ranges between 2.84 °C and 30.10 °C. The average daily LST values range from -8.3342 °C to 8.4248 °C for normal days, and it is equal to 13.456 °C for the anomalous day on September 25, 2019 (a night after the EQ). Fig. 8(b) shows that the deviations range from 0.0016 °C to 1.4828 °C. The maximum and minimum deviations are equal to 3.5114 °C and 0.00739 °C, respectively.

B. Discussion

In this article, we observed significant ionospheric anomalies triggered by the continuous emission of radon from the EQ breeding zone as reported by Pulinets and Ouzounov [6] and Pulinets [23]. Besides, the ionosphere can be disturbed by the air variation over the epicenter, which is caused by tectonic forces and squeeze rocks leading to the emission of p-holes [16]. This article offers an adequate evidence for atmospheric anomalies in the form of thermal variation followed by the ionospheric irregularities over the epicenter. During the main shock day, the thermal anomalies observed in the ionosphere over the seismogenic zone are caused by lithosphere-iono-sphere coupling. The EQ-induced thermal anomalies are activated from tectonic plates and stress of the tectonic plates in which they lead to a massive release of energy and a prime phase for the EQ preparation. The GPS values obtained from the continuous observations of the GPS satellites indicate the anomalies consistency of VTEC and dTEC time series. Diurnal variation in temporal TEC pronounces the thermal anomalies after the Pakistan EQ within 5 days beyond the upper bound over the seismogenic zone, as displayed in Fig. 1. This article portrays the lithospheric attribute around EQ epicenter in atmosphere and ionosphere, however, further investigation in other regions over the globe can be conducted additionally to explain and support the discovered phenomena.

V. CONCLUSION

In this article, the thermal and ionospheric anomalies from MODIS LST, GPS TEC, and GIM TEC are investigated as possible EQ precursors for the M$_w$ 5.6 Pakistan EQ. The main findings are summarized as follows.

1) TEC anomalies of Sukkur GPS station and GIMs are prominent from the rest of the measurement above the upper confidence bound on September 25, 2019 (one day after the main shock day). It demonstrates a variation of more than 5 TECU during 1000–1400 LT on September 25, 2019 over the epicenter for the completion of LAIC mechanism.

2) Daytime LST values obtained from statistical calculation and ANN-based prediction show no enhancement before and after the main shock day, which shows the existence of no abnormality over the epicenter during daytime LST clouds. On the other hand, the low intense LST value with

less than 1°C after more than a month of the main shock day suggests that it is no bona fide EQ anomaly.

3) An abnormal rise in LST of about 17.68 °C observed in the nighttime LST immediately after the EQ day (on September 25, 2019) in spatial TEC maps and temporal TEC time series. Nighttime LST anomaly is also verified by the ANN procedure by which the predicted temperatures range from 2.8 °C to 13.4 °C after the main shock day. The overall nighttime analysis shows that an emanation of 2.9 °C–20.6 °C exists in the surface temperature leading to the execution of atmosphere anomalies in LAIC coupling.

All these anomalies after the EQ based on multiple satellite observations assist in the developments of LAIC hypothesis for seismic precursors. However, more analyses with different data types and studies are still required to enhance more knowledge in the field of EQ precursors.

REFERENCES

[1] A. Sekertekin, S. Inyurt, and S. Yaprak, "Pre-seismic ionospheric anomalies and spatio-temporal analyses of MODIS Land surface temperature and aerosols associated with Sep, 24 2013 Pakistan Earthquake," *J. Atmospheric Solar-Terr. Phy.*, vol. 200, 2020, Art. no. 105218.

[2] M. Shah *et al.*, "Total electron content anomalies associated with earthquakes occurred during 1998–2019," *Acta Astronaut.*, vol. 175, pp. 268–276, 2020.

[3] A. A. Tronin, "Satellite Remote Sensing in Seismology. A Review," *Remote Sens.*, vol. 2, no. 1, pp. 124–150, 2010.

[4] M. Bellaoui, A. Hassini, and K. Bouchouicha, "Pre-seismic anomalies in remotely sensed land surface temperature measurements: The case study of 2003 Boumerdes earthquake," *Adv. Space Res.*, vol. 59, no. 10, pp. 2645–2657, 2017.

[5] F. Freund, G. Ouillon, J. Scoville, and D. Sornette, "Earthquake precursors in the light of proxy defects theory: critical review of systematic observations," *Eur. Phys. J.*, vol. 230, pp. 1–56, 2017.

[6] S. Pulinets and D. Ouzounov, "Lithosphere–Atmosphere–Ionosphere Coupling (LAIC) model – An unified concept for earthquake precursors validation," *J. Asian Earth Sci.*, vol. 41, no. 1/2, pp. 371–382, 2011.

[7] S. Inyurt, S. Peker, and C. Mekik, "Monitoring potential ionospheric changes caused by Van earthquake (Mw 7.2)," *Ann. Geophys.*, vol. 37, no. 2, pp. 143–151, 2019.

[8] M. Ulukavak and S. Inyurt, "Seismo-ionospheric precursors of strong sequential earthquakes in Nepal region," *Acta Astronaut.*, vol. 166, pp. 123–130, 2020.

[9] A. K. Saraf *et al.*, "Satellite detection of earthquake thermal infrared precursors in Iran," *Nat. Hazards*, vol. 47, no. 1, pp. 119–35, 2008.

[10] S. A. Khan, K. Pilakoutas, I. Hajirasouliha, R. Garcia, and M. Guadagnini, "Seismic risk assessment for developing countries: Pakistan as a case study," *Earthquake Eng. Eng. Vib.*, vol. 17, pp. 787–804, 2018.

[11] M. R. Khan, F. Hameed, M. S. Mughal, M. Basharat, and S. Mustafa, "Tectonic Study of the Sub-Himalayas Based on Geophysical Data in Azad Jammu and Kashmir and Northern Pakistan," *J. Earth Sci.*, vol. 27, pp. 981–988, 2016.

[12] Z. Wan and Z. L. Li, "A physics-based algorithm for retrieving land-surface emissivity and temperature from EOS/MODIS data," *IEEE Tran. Geosci. Remote Sens.*, vol. 35, no. 4, pp. 980–996, Jul. 1997.

[13] I. R. Dobrovolsky, S. I. Zubkov, and V. I. Myachkin, "Estimation of the Size of Earthquake Preparation Zones," *Pure Appl. Geophys.*, vol. 117, pp. 1025–1044, 1979.

[14] S. Muster, M. Langer, A. Abnizova, K. L. Young, and J. Boike, "Spatio-temporal sensitivity of MODIS land surface temperature anomalies indicates high potential for large-scale land cover change detection in Arctic permafrost landscapes," *Remote Sens. Environ.*, vol. 168, pp. 1–12, 2015.

[15] M. Shah, R. U. Qureshi, N. G. Khan, M. Ehsan, and J. Yan, "Artificial Neural Network based thermal anomalies associated with earthquakes in Pakistan from MODIS LST," *J. Atmospheric Solar-Terr. Phy.*, vol. 215, 2021, Art. no. 105568.

[16] F. Freund *et al.*, "Air ionization at rock surface and pre-earthquake signals," *J. Atmospheric Solar-Terr. Phy.*, vol. 71, pp. 1824–1834, 2009.

[17] G. C. Hulley, C. Ghent, F. M. Göttsche, P. C. Guillevic, D. J. Mildrexler, and C. Coll, *Land Surface Temperature.* Amsterdam, Netherlands: Elsevier, 2019, pp. 57–127.

[18] A. A. Tronin, M. Hayakawa, and O. A. Molchanov, "Thermal IR satellite data application for earthquake research in Japan and China," *J. Geodyn.*, vol. 33, no. 4/5, pp. 519–534, 2002.

[19] D. Ouzounov, N. Bryant, C. Filizzola, N. Pergola, P. Taylor, and V. Tramutoli, "Advances in analysis of pre-earthquake thermal anomalies by analyzing IR satellite data," in *Proc. 35th COSPAR Scientific Assem. Paris, France*, 2004, Art. no. 3035.

[20] M. A. Dunajecka and S. A. Pulinets, "Atmospheric and thermal anomalies observed around the time of strong earthquakes in Mexico," *Atmosfera*, vol. 18, no. 4, pp. 233–247, 2005.

[21] S. A. Pulinets *et al.*, "Thermal, atmospheric and ionospheric anomalies around the time of the Colima M7.8 earthquake of 21 January 2003," *Ann. Geophys.*, vol. 24, pp. 835–849, 2006.

[22] J. Ma, S. Chen, X. Hu, P. Liu, and L. Liu, "Spatial-temporal variation of the land surface temperature field and present-day tectonic activity," *Geosci. Frontiers*, vol. 1, no. 1, pp. 57–67, 2010.

[23] S. A. Pulinets, "Physical mechanism of the vertical electric field generation over active tectonic faults," *Adv. Space Res.*, vol. 44, pp. 767–773, 2009.

[24] W. Zhao, S. B. Duan, A. Li, and G. Yin, "A practical method for reducing terrain effect on land surface temperature using random forest regression," *Remote Sens. Environ.*, vol. 221, pp. 635–649, 2019.

[25] W. Zhao and S. B. Duan, "Reconstruction of daytime land surface temperatures under cloud-covered conditions using integrated MODIS/Terra land products and MSG geostationary satellite data," *Remote Sens. Environ.*, vol. 247, 2020, Art. no. 111931.

[26] E. K. Mohamed, V. K. Gahalaut, A. Sekertekin, and S. Inyurt, "Atmospheric, ionospheric and earth-related variations associated with the 11th August 2012 earthquakes, Ahar, Iran," *J. Atmos. Sol. Terr. Phys.*, vol. 216, 2021, Art. no. 105595.

[27] Z. Wan, S. Hook, and G. Hulley, "MOD11A1 MODIS/Terra Land Surface Temperature/Emissivity Daily L3 Global 1 km SIN Grid V006," NASA EOSDIS LP DAAC; NASA: Washington, DC, USA, 2015.

[3][Online]. Available: https://earthquake.usgs.gov/earthquakes/search/

[4][Online]. Available: https://www.intermagnet.org

[5][Online]. Available: https://cddis.nasa.gov/

[6][Online]. Available: https://www.iba-suk.edu.pk/faculty/details/INS-0091

Amna Hafeez is currently working toward the graduate degree with the Department of GNSS, Institute of Space Technology, Islamabad, Pakistan.

Her research interests include the analyses about lithosphere-atmosphere-ionosphere coupling associated with the earthquake based on MODIS LST, GPS TEC, and GIM TEC.

Munawar Shah received the master's degree in geophysics from Quaid e Azam University, Islamabad, Pakistan, in 2013 and the Ph.D. degree in geodesy and geodynamics from Shanghai Astronomical Observatory, Chinese Academy of Sciences, Beijing, China, in 2017.

Since 2017, he has been an Assistant Professor with the Department of GNSS, Institute of Space Technology, Islamabad, Pakistan. His research interests include GNSS ionospheric modeling and earthquake investigation based on artificial neural network and statistical methods.

Muhsan Ehsan, photograph and biography not available at the time of publication.

Punyawi Jamjareegulgarn received the Ph.D. degree from the Department of Telecommunication Engineering, King Mongkut's Institute of Technology Ladkrabang, Bangkok, Thailand, in 2017.

Since 2012, he has been an Assistant Professor with the Department of Engineering, King Mongkut's Institute of Technology Ladkrabang, Prince of Chumphon Campus, Chumphon, Thailand.

His research interests include ionospheric irregularities, TEC modeling, RTK-based positioning and multi-GNSS signals, plasma bubbles, and earthquake investigations based on GPS TEC and GIM TEC.

Junaid Ahmed, photograph and biography not available at the time of publication.

M. Arslan Tariq, photograph and biography not available at the time of publication.

Shahid Iqbal, photograph and biography not available at the time of publication.

Najam Abbas Naqvi, photograph and biography not available at the time of publication.